American Mineralogist, Volume 84, pages 555–563, 1999

In-situ neutron diffraction study of non-convergent cation ordering in the $(Fe_3O_4)_{1-x}(MgAl_2O_4)_x$ spinel solid solution

RICHARD J. HARRISON,[1,*] MARTIN T. DOVE,[2] KEVIN S. KNIGHT,[3] AND ANDREW PUTNIS[1]

[1]Institut für Mineralogie, Universität Münster, Corrensstrasse 24, 48149 Münster, Germany
[2]Department of Earth Sciences, University of Cambridge, Downing Street, Cambridge CB2 3EQ, U.K.
[3]Rutherford Appleton Laboratories, Oxfordshire OX11 OQX, U.K.

ABSTRACT

Non-convergent cation ordering in the $(Fe_3O_4)_{1-x}(MgAl_2O_4)_x$ solid solution was investigated using in-situ time-of-flight neutron powder diffraction. The approach to equilibrium in a sample with $x = 0.75$ was observed at 923 K by performing in-situ structure refinements at intervals of 5 min, and the ordering behavior was traced through the time-dependence of the lattice parameter, the cation-oxygen bond lengths, and the cation-site scattering lengths. The data are consistent with a two-stage kinetic process in which relatively rapid exchange of Fe^{3+} with Mg and Fe^{2+} between tetrahedral and octahedral sites was followed by slower exchange of Mg with Al. The Fe^{3+} cations are shown to order onto tetrahedral sites, contrary to the predictions of thermodynamic models for the solid solution.

Equilibrium cation distributions in samples with $x = 0.4$, 0.5, and 0.75 were determined between 1073 and 1273 K by combining the structure refinements with measurements of saturation magnetization in quenched material. The adopted cation distribution was a compromise between the normal and inverse distributions observed in the end-members. The conflict of site preference between these two ordering schemes resulted in a simple behavior in the middle of the solid solution in which Al occurred predominantly on octahedral sites and the Mg, Fe^{2+}, and Fe^{3+} cations were distributed randomly over the remaining sites. The ordering scheme adopted away from the middle of the solid solution was obtained by combining this pseudo-random scheme with a tetrahedral site preference of Fe^{3+} relative to Mg and Fe^{2+}. Comparison of the structure refinements with published thermodynamic models demonstrates that quantitative agreement was poor between calculated and observed behavior in this system. Qualitative agreement with the O'Neill-Navrotsky thermodynamic model was found near the middle of the solid solution.

INTRODUCTION

The 2-3 class of oxide spinels (space group $Fd\bar{3}m$) is represented by the general formula unit AB_2O_4 where A is a divalent cation and B is a trivalent cation. The oxygen anions form an approximately cubic close packed arrangement, and the cations distribute themselves over one tetrahedral site and two octahedral sites per formula unit, according to the general scheme:

$$A_{1-i}B_i\left(A_{\frac{i}{2}}B_{1-\frac{i}{2}}\right)_2O_4$$

where brackets represent cations on octahedral sites. The variable i is referred to as the inversion parameter. Two ordered configurations of the spinel structure can be adopted at low temperatures; the normal configuration with $i = 0$ and the inverse configuration with $i = 1$. At elevated temperatures, the cations became increasingly randomly distributed over tetrahedral and octahedral sites. A value of $i = 2/3$ corresponded to a completely random distribution of A and B over the three cation sites per formula unit. Because the order-disorder process in spinel is of the non-convergent type (there is no symmetry difference between an ordered and a totally disordered spinel), such a completely random distribution would only be anticipated at infinite temperature and is approached asymptotically on increasing temperature.

The end-members magnetite (Fe_3O_4) and spinel ($MgAl_2O_4$) adopt the inverse and normal cation distributions respectively at low temperature (Millard et al. 1992; Peterson et al. 1991; Wood et al. 1986; Wu and Mason 1981). Cation ordering in their solid solutions is expected to be a complex function of composition, due to the conflict of site preference displayed by Mg and Fe^{2+} cations in the end-members (O'Neill and Navrotsky 1984). Experimental determination of the ordering is made difficult by several factors. First, the experiments have to be performed in situ, due to the unavoidable problem of cation redistribution during quenching from high temperature (Wood et al. 1986; Millard et al. 1992; Larsson et al. 1994; Harrison and Putnis 1996). This is especially a problem in spinels containing Fe^{2+} and Fe^{3+} cations, because these can exchange with each other relatively rapidly by the transfer of an electron. Second, the experiments have to be performed either under high vacuum or controlled oxygen fugacity to prevent oxidation of Fe^{2+} to Fe^{3+}. Finally, because of many independent variables needed to describe the cation distribution, a combination of several inde-

*E-mail: harrisr@nwz.uni.muenster.de

0003-004X/99/0004–0555$05.00

pendent experimental observations is required to obtain unique values for all the cation occupancies.

The difficulty in determining cation distributions experimentally prompted several theoretical studies of cation ordering in this system (O'Neill and Navrotsky 1984; Lehmann and Roux 1984; Nell and Wood 1989; Sack and Ghiorso 1991). These models allow calculation of the cation distribution as a function of temperature and composition and are commonly used to ascertain oxygen fugacities in the upper mantle (O'Neill and Wall 1987; Woodland 1988; Wood 1990). To date, only one in-situ study exists with which to test these theoretical models: Nell et al. (1989) which measured in-situ cation distributions using the electrical conductivity/Seebeck-effect technique (Mason 1987). We demonstrate in this study, however, that inconsistencies exist between the experimental measurements of Nell et al. (1989) and the saturation magnetization measurements of Harrison and Putnis (1995) and Harrison (1997).

This study aims to provide a new experimental constraint on the cation ordering in the $(Fe_3O_4)_{1-x}(MgAl_2O_4)_x$ solid solution through in-situ structure refinements using time-of-flight neutron powder diffraction (Peterson et al. 1991; Redfern et al. 1996). Time-of-flight neutron scattering is an ideal probe of cation ordering in this mineral, due to the good contrast between the neutron scattering lengths of Fe, Mg, and Al (Table 1), the ability to perform the experiment in-situ under high vacuum, and the ability to record the entire diffraction pattern rapidly (hence reducing the amount of time the sample was annealed at high temperature, which lowers the probability of exsolution occurring at temperatures below 1000 °C). Although the data did not allow the specific distribution of Mg, Al, Fe^{2+}, and Fe^{3+} to be calculated uniquely, the high accuracy and precision of the results permitted evaluation of various thermodynamic theories of the cation ordering process. With appropriate assumptions, we propose a simple cation ordering scheme that is consistent with both the in-situ structure refinements and the measurements of saturation magnetization in quenched material.

EXPERIMENTAL PROCEDURES

Sample synthesis

Samples of the $(Fe_3O_4)_{1-x}(MgAl_2O_4)_x$ solid solution with x = 0.4, 0.5, and 0.75 were synthesized from the oxides using the technique described by Harrison and Putnis (1995). The starting materials for all syntheses were 99.9% pure Fe_2O_3 and MgO, and Al_2O_3 prepared by firing $AlCl_3 \cdot 6H_2O$ for 2 h at 673 K, 5 h at 973 K, and 1 h at 1173 K. The oxides were weighed in stoichiometric proportions, ground together, and pressed into pellets of 13 mm radius and thickness 2 to 4 mm. Five pellets at a time were then suspended in a platium-wire basket (to minimize the contact between the Pt and the sample) and fired at 1673 K for 24 h in a vertical-tube gas-mixing furnace under controlled oxygen fugacity (Nafziger et al. 1971). A value of $\log(f_{O_2}) = -4.2$ was chosen to yield stoichiometry in the magnetite component of the solid solution (Dieckmann 1982). Samples were quenched from 1673 K by dropping directly from the furnace into water. Each batch of five pellets was then ground together and fired for an additional 24 h under the same conditions. The samples were then examined using a Phillips X-ray diffractometer. All samples were single-phase spinels with sharp peaks. No trace of unreacted oxides were found in either the X-ray traces or in the subsequent neutron diffraction experiments. Compositions of the samples were checked using electron microprobe analysis on a CAMECA SX50 using an energy dispersive detector (Table 2).

TABLE 1. Individual scattering lengths and room temperature tetrahedral-oxygen bond lengths

Cation	b (fm)	R_{tet} (Å)†
Mg	5.375	1.965
Al	3.449	1.77
Fe^{2+}	9.45	1.995
Fe^{3+}	9.45	1.865

*Sears (1992).
†From O'Neill and Navrotsky (1983).

Neutron diffraction procedures

The neutron powder diffraction data were collected using the high-intensity POLARIS time-of-flight diffractometer at the ISIS spallation neutron source (Rutherford Appleton Laboratory, U.K.). The sample powder was loaded into a thin-walled vanadium can and suspended inside a vanadium element furnace, which was evacuated to a pressure of 10^{-6} mbar. The temperature was measured and controlled using type K thermocouples. The sample and furnace thermal mass ensured good thermal stability throughout each data collection. The neutron diffraction patterns were collected for flight times between 2.5 and 19.6 ms, corresponding to d-spacings between 0.4 and 3.2 Å. This range of data included around 250 independent Bragg reflections, giving 140 individual Bragg peaks in the powder diffraction pattern when accounting for different reflections having identical d-spacings. The data from individual detectors were corrected for electronic noise, normalized against standard spectra from a sample of vanadium, and focused using in-house software. No corrections were made for beam attenuation by the furnace or sample, because these were found to be negligible.

The crystal structures were refined from the data using the Rietveld method with in-house software. The background signal was modeling using Chebyshev polynomials. The crystallographic variables were the unit cell parameters, the coordinates of the O atoms, the occupancies of the tetrahedral and octahedral sites, and the temperature factors (space group $Fd\bar{3}m$). The site occupancies were handled by refining the neutron scattering length associated with each site, subject to the constraint that the sum of the scattering lengths should remain at a constant value. The anisotropic temperature factors of the oxygen sites were refined using two independent parameters, but it was found that no improve-

TABLE 2. Microanalysis of synthetic samples

Sample	Mg (mol%)	Al (mol%)	Fe (mol%)	O (mol%)	Mg	Al	Fe	Sum
NS75	10.9(2)	21.6(2)	10.7(2)	56.7	0.77(7)	1.52(9)	0.76(10)	3.05
NS50	6.9(1)	13.7(2)	22.2(2)	57.2	0.48(6)	0.96(9)	1.55(10)	2.99
NS40	5.4(1)	11.1(2)	26.2(3)	57.22	0.38(7)	0.8(1)	1.8(1)	2.98

ment in the refinement could be obtained using anisotropic temperature factors for the atoms on the octahedral and tetrahedral sites, so these were treated using isotropic temperature factors. All three samples were paramagnetic at the temperatures investigated, and hence there were no contributions due to magnetic scattering in the diffraction patterns. An example of a fitted diffraction pattern is given in Figure 1, and the results of the refinements are listed in Table 3.

RESULTS AND DISCUSSION

Ordering behavior during isothermal annealing

As mentioned earlier, the cation distribution partially reorders during quenching until it becomes frozen-in below some closure temperature. If this quenched material is annealed below the closure temperature there is a thermodynamic driving force for ordering, and the cations attempt to move onto their preferred sites (Redfern et al. 1996). The way in which the $(Fe_3O_4)_{1-x}(MgAl_2O_4)_x$ solid solution approached equilibrium was investigated at 923 K and composition $x = 0.75$ by annealing the sample in the diffractometer and performing in-situ structure refinements as a function of time. The relatively high neutron flux of the POLARIS diffractometer and the ability to collect the whole diffraction pattern at once allowed structure refinements to be obtained with a counting time of 5 min. This counting time was a satisfactory compromise between obtaining good counting statistics and minimizing error due to the change in the cation distribution with time. At this bulk composition and temperature, the system lies outside the coherent solvus. Although incoherent exsolution is thermodynamically feasible under these conditions, no evidence of exsolution was seen in the diffraction patterns.

The variation in the lattice parameter (a) as a function of annealing time for the composition $x = 0.75$ is shown in Figure 2a. During the first 1400 s of the measurement, a sharply increased, after which a increases at a very much slower rate. This slowing down in the rate of change of a is often interpreted as the cation distribution approaching equilibrium. This is not the case here as shown by the corresponding changes in tetrahedral and octahedral site bond length (R_{tet} and R_{oct}) during the experiment (Figs. 2b and 2c). Although the error bars are large (due to the short counting times), significant changes in R_{tet} and R_{oct} clearly occurred between 1400 and 4000 s. Despite the very small changes in a during this period, cation exchange between tetrahedral and octahedral sites was still occurring, and the sample had not reached equilibrium.

One possible explanation for the lattice parameter behavior can be obtained by treating the data obtained during the first 1400 s (stage 1) separately from the data obtained subsequently (stage 2). The sharp increase in a during stage 1 was accompanied by a small decrease in R_{tet} and a small increase in R_{oct}, whereas the slow increase in a during stage 2 is accompanied by an increase in R_{tet} and a decrease in R_{oct}. Simultaneously, the tetrahedral site scattering length (b_{tet}) very slightly increases during stage 1, after which b_{tet} remains essentially constant. These observations suggest that each of the two stages is associated with a different cation exchange reaction (or combination of reactions). Because mobilities of the various cations in the solid solution can be very different, it is possible for the system to reach various intermediate equilibrium states during annealing where each intermediate state is defined by minimizing the free energy of ordering with respect to some, but not all, of the cation occupancies (Sha and Chappell 1996). When an intermediate state is approached, the cation exchange process responsible for reaching that state slows down, and the other cation exchange processes continues until the next state of equilibrium is reached. This leads to a changeover of the dominant cation exchange reaction and hence a change in the trends of a, R_{tet}, R_{oct}, and b_{tet} vs. time.

The dominant cation exchange reactions responsible for the two stages of the isothermal annealing experiment can be determined using Table 4, which summarizes the changes in R_{tet} and b_{tet} for the six possible cation exchange reactions (the additional six reverse reactions are not germain). The decrease in R_{tet} and increase in b_{tet} during stage 1 is consistent with the first two cation

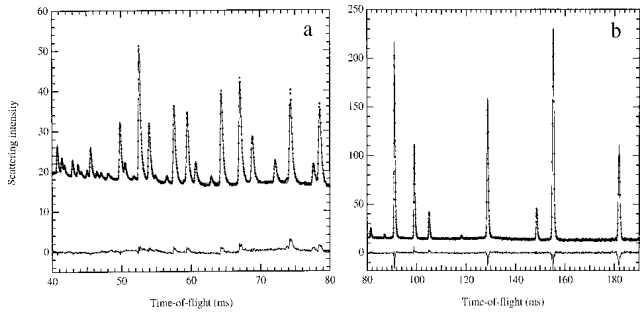

FIGURE 1. Time-of-flight neutron diffraction pattern for synthetic spinel. There is a linear relationship between time-of-flight and the interplanar d-spacing. In this case, the limits correspond to (**a**) 0.65–1.3 Å, and (**b**) 1.3–3.17 Å.

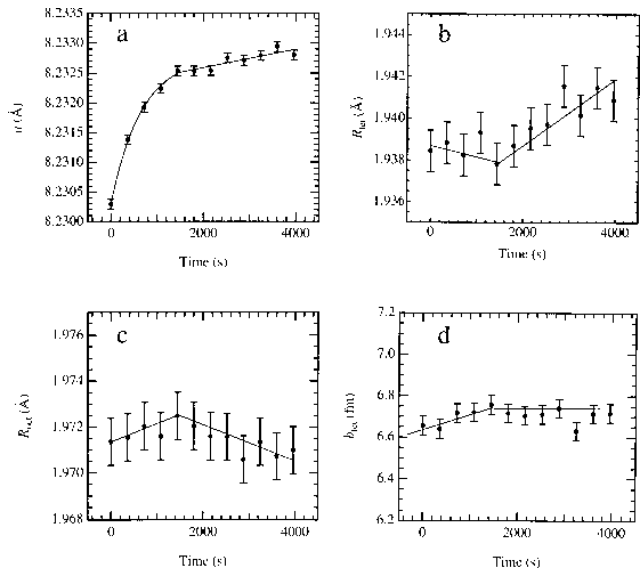

FIGURE 2. Time dependence of (**a**) lattice parameter, (**b**) tetrahedral-oxygen bond length, (**c**) octahedral-oxygen bond length, and (**d**) tetrahedral scattering length during isothermal annealing at 923 K and $x = 0.75$. Solid lines are guides to the eye.

TABLE 3. Results of structure refinements

X	T (K)	a (Å)	μ	B_{tet} (fm)	R_{tet} (Å)	R_{oct} (Å)	B_{tet}	B_{oct}	Time (s)
0.4	873	8.34380(2)	0.25929(4)	8.51(3)	1.9407(6)	2.0114(6)	1.05(2)	0.779(2)	
0.4	923	8.34863(2)	0.25933(4)	8.53(3)	1.9424(6)	2.0123(6)	1.12(2)	0.816(2)	
0.4	973	8.35362(2)	0.25942(4)	8.49(3)	1.9449(6)	2.0128(6)	1.17(2)	0.893(2)	
0.4	1023	8.35932(2)	0.25960(4)	8.55(3)	1.9488(6)	2.0128(6)	1.26(2)	0.942(2)	
0.4	1073	8.36430(2)	0.25958(4)	8.55(3)	1.9497(6)	2.0141(6)	1.33(2)	0.979(2)	
0.4	1123	8.36931(2)	0.25957(4)	8.55(3)	1.9507(6)	2.0154(6)	1.39(2)	1.030(2)	
0.4	1173	8.37430(2)	0.25957(4)	8.54(3)	1.9519(6)	2.0166(6)	1.46(2)	1.071(2)	
0.4	1223	8.37944(2)	0.25960(4)	8.50(3)	1.9535(6)	2.0176(6)	1.53(2)	1.127(2)	
0.4	1273	8.38412(2)	0.25955(4)	8.50(3)	1.9539(6)	2.0191(6)	1.62(2)	1.186(2)	
0.4	1173	8.37466(2)	0.25963(4)	8.57(3)	1.9529(6)	2.0162(6)	1.46(2)	1.066(2)	
0.4	1073	8.36514(2)	0.25964(4)	8.59(3)	1.9508(6)	2.0139(6)	1.33(2)	0.961(2)	
0.5	873	8.31646(2)	0.25985(4)	7.94(3)	1.9425(6)	2.0006(6)	1.04(2)	0.909(2)	
0.5	898	8.31887(2)	0.25984(4)	7.96(3)	1.9429(6)	2.0012(6)	1.08(2)	0.924(2)	
0.5	923	8.32133(2)	0.25979(4)	7.95(3)	1.9427(6)	2.0022(6)	1.12(2)	0.945(2)	
0.5	948	8.32381(2)	0.25983(4)	7.94(3)	1.9439(6)	2.0025(6)	1.13(2)	0.988(2)	
0.5	973	8.32629(2)	0.25988(4)	7.97(3)	1.9452(6)	2.0027(6)	1.19(2)	0.986(2)	
0.5	998	8.32876(2)	0.25996(4)	7.95(3)	1.9469(6)	2.0027(6)	1.20(2)	1.020(2)	
0.5	1023	8.33129(2)	0.25995(4)	7.94(3)	1.9474(6)	2.0034(6)	1.24(2)	1.050(2)	
0.5	1048	8.33387(2)	0.26001(4)	7.96(3)	1.9488(6)	2.0035(6)	1.27(2)	1.060(2)	
0.5	1073	8.33639(2)	0.26008(4)	7.99(3)	1.9504(6)	2.0036(6)	1.31(2)	1.080(2)	
0.5	1098	8.33872(2)	0.26005(4)	7.97(3)	1.9505(6)	2.0044(6)	1.33(2)	1.100(2)	
0.5	1123	8.34105(2)	0.26000(4)	7.94(3)	1.9504(6)	2.0053(6)	1.34(2)	1.130(2)	
0.5	1148	8.34339(2)	0.25999(4)	7.95(3)	1.9508(6)	2.0060(6)	1.41(2)	1.170(2)	
0.5	1173	8.34569(2)	0.25998(4)	7.94(3)	1.9512(6)	2.0066(6)	1.44(2)	1.180(2)	
0.5	1198	8.34803(2)	0.25997(4)	7.91(3)	1.9516(6)	2.0072(6)	1.44(2)	1.230(2)	
0.5	1223	8.35039(2)	0.25997(4)	7.93(3)	1.9521(6)	2.0078(6)	1.49(2)	1.240(2)	
0.5	1248	8.35268(2)	0.25992(4)	7.92(3)	1.9519(6)	2.0087(6)	1.54(2)	1.260(2)	
0.5	1273	8.35495(2)	0.25993(4)	7.89(3)	1.9526(6)	2.0092(6)	1.56(2)	1.310(2)	
0.5	1173	8.34556(2)	0.26004(4)	7.94(3)	1.9520(6)	2.0061(6)	1.43(2)	1.180(2)	
0.5	1073	8.33628(2)	0.26012(4)	8.01(3)	1.9510(6)	2.0033(6)	1.30(2)	1.070(2)	
0.75	923	8.23029(8)	0.26098(7)	6.66(5)	1.938(1)	1.971(1)			0(10)
0.75	923	8.23138(8)	0.26099(7)	6.64(5)	1.939(1)	1.972(1)			360(10)
0.75	923	8.23192(8)	0.26094(7)	6.72(5)	1.938(1)	1.972(1)			720(10)
0.75	923	8.23224(8)	0.26101(7)	6.72(5)	1.939(1)	1.972(1)			1080(10)
0.75	923	8.23253(8)	0.26090(7)	6.76(5)	1.938(1)	1.972(1)			1440(10)
0.75	923	8.23253(8)	0.26096(7)	6.72(5)	1.939(1)	1.972(1)			1800(10)
0.75	923	8.23254(8)	0.26102(7)	6.70(5)	1.940(1)	1.972(1)			2160(10)
0.75	923	8.23275(8)	0.26103(7)	6.71(5)	1.940(1)	1.972(1)			2520(10)
0.75	923	8.23271(8)	0.26116(7)	6.74(5)	1.942(1)	1.971(1)			2880(10)
0.75	923	8.23279(8)	0.26106(7)	6.63(5)	1.940(1)	1.971(1)			3240(10)
0.75	923	8.23294(8)	0.26115(7)	6.71(5)	1.942(1)	1.971(1)			3600(10)
0.75	923	8.23280(8)	0.26111(7)	6.72(5)	1.941(1)	1.971(1)			3960(10)
0.75	938	8.23390(2)	0.26113(4)	6.72(3)	1.9414(6)	1.9711(6)			
0.75	953	8.23544(2)	0.26111(4)	6.73(3)	1.9415(6)	1.9716(6)			
0.75	968	8.23681(2)	0.26111(4)	6.73(3)	1.9418(6)	1.9719(6)			
0.75	983	8.23816(2)	0.26103(4)	6.74(3)	1.9410(6)	1.9729(6)			
0.75	998	8.23935(2)	0.26117(4)	6.75(3)	1.9433(6)	1.9721(6)			
0.75	1013	8.24059(2)	0.26111(4)	6.71(3)	1.9427(6)	1.9729(6)			
0.75	1028	8.24186(2)	0.26112(4)	6.77(3)	1.9432(6)	1.9731(6)			
0.75	1043	8.24310(2)	0.26115(4)	6.74(3)	1.9439(6)	1.9732(6)			
0.75	1058	8.24436(2)	0.26110(4)	6.75(3)	1.9435(6)	1.9738(6)			
0.75	1073	8.24573(2)	0.26108(4)	6.75(3)	1.9435(6)	1.9743(6)			
0.75	1088	8.24702(2)	0.26106(4)	6.73(3)	1.9435(6)	1.9748(6)			
0.75	1103	8.24828(2)	0.26115(4)	6.72(3)	1.9451(6)	1.9744(6)			
0.75	1118	8.24972(2)	0.26108(4)	6.71(3)	1.9444(6)	1.9753(6)			
0.75	1133	8.25120(2)	0.26111(4)	6.70(3)	1.9452(6)	1.9754(6)			
0.75	1148	8.25259(2)	0.26115(4)	6.76(3)	1.9461(6)	1.9754(6)			
0.75	1163	8.25402(2)	0.26115(4)	6.77(3)	1.9465(6)	1.9758(6)			
0.75	1178	8.25525(2)	0.26110(4)	6.74(3)	1.9460(6)	1.9764(6)			
0.75	1193	8.25664(2)	0.26111(4)	6.75(3)	1.9465(6)	1.9767(6)			
0.75	1208	8.25782(2)	0.26104(4)	6.71(3)	1.9458(6)	1.9775(6)			
0.75	1223	8.25901(2)	0.26098(4)	6.71(3)	1.9452(6)	1.9782(6)			
0.75	1238	8.26002(2)	0.26095(4)	6.68(3)	1.9450(6)	1.9787(6)			
0.75	1253	8.26120(2)	0.26091(4)	6.70(3)	1.9447(6)	1.9793(6)			
0.75	1263	8.26189(2)	0.26091(4)	6.67(3)	1.9449(6)	1.9794(6)			
0.75	1273	8.26270(2)	0.26095(4)	6.64(3)	1.9456(6)	1.9793(6)			
0.75	1223	8.25836(2)	0.26101(4)	6.73(3)	1.9455(6)	1.9779(6)			
0.75	1173	8.25410(2)	0.26108(4)	6.76(3)	1.9455(6)	1.9763(6)			
0.75	1123	8.24985(2)	0.26105(4)	6.70(3)	1.9440(6)	1.9755(6)			
0.75	1073	8.24569(2)	0.26114(4)	6.74(3)	1.9444(6)	1.9739(6)			
0.75	1023	8.24145(2)	0.26112(4)	6.70(3)	1.9431(6)	1.9730(6)			
0.75	973	8.23735(2)	0.26115(4)	6.71(3)	1.9425(6)	1.9718(6)			

Notes: Space group $Fd\bar{3}m$.

exchange reactions in Table 4, both of which involve Fe^{3+} cations ordering onto tetrahedral sites, displacing Mg and Fe^{2+} cations onto octahedral sites. The time taken to reach this state agrees well with experimental data on the rate of Mg-Fe^{3+} exchange in $MgFe_2O_4$ (O'Neill 1994). The increase in R_{tet} during stage 2 of the ordering is consistent with any of the other four forward reactions in Table 4. The negligible increase in b_{tet} suggests that the most appropriate reaction involves Al cations ordering onto octahedral sites, displacing Mg cations onto tetrahedral sites.

The reason that the change in a during stage 2 is smaller than in stage 1, despite the fact that the change in R_{tet} is larger, can be seen by examining the relationship between cell parameter and bond length:

$$a = \frac{40R_{tet} + 8\sqrt{33R_{oct}^2 - 8R_{tet}^2}}{11\sqrt{3}} \quad (1)$$

Equation 1 is plotted as a contour diagram in Figure 3. The solid arrows show the observed paths taken by R_{tet} and R_{oct} during the annealing experiment (obtained by plotting the solid lines in Figs. 2b and 2c against each other). The exchange of Fe^{3+} with Mg and Fe^{2+} during the first stage causes the system to cut across the contours, leading to a large change in a. The exchange of Al with Mg during the second stage causes the system to move approximately parallel to the contours, leading to a much smaller increase in a. Thus, measurements of a alone gives a false impression that the cation distribution is approaching equilibrium. In solid solutions where different cation exchange processes occur at different rates, more detailed measurements are required to distinguish between the various states of intermediate and global equilibrium.

Alternatively, increasing lattice parameter can be explained by a change in the oxidation state of the sample as it is annealed under vacuum (R.C. Peterson, personal communication). The rapid increase in lattice parameter is consistent with conversion of Fe^{3+} to Fe^{2+} as the sample adjusts to the new redox conditions of the annealing experiment. The rate of change of a decreases as the sample approaches the equilibrium Fe^{2+}/Fe^{3+} ratio for the new oxygen fugacity. This explanation is consistent with the overall rate of increase in a and the small change in b_{tet} observed during annealing. We feel, however, that it is not consistent with the observed changes in bond length during annealing (Figs. 2b, 2c, and 3). We demonstrate in the next section that Fe^{3+} occurs in approximately equal proportions on tetrahedral and octahedral sites in this sample at this annealing temperature. Therefore, if the increase in a is caused by the reduction of Fe^{3+} to Fe^{2+}, one would expect both R_{tet} and R_{oct} to increase in the manner shown by the dotted arrow in Figure 3, rather than in the observed manner (shown by the solid arrows). Furthermore, one would expect the increase in bond length to be rapid at first and slow down as the sample reached equilibrium. Because the opposite is observed during annealing, we favor the interpretation presented above based on the exchange of cations between tetrahedral and octahedral sites.

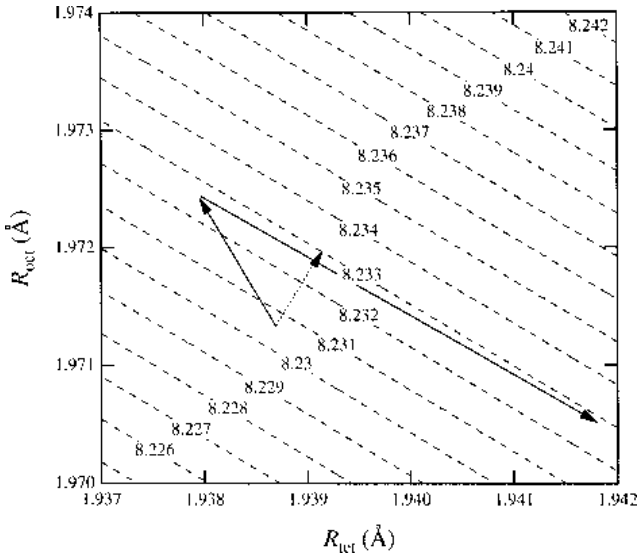

FIGURE 3. Contour diagram illustrating the relationship between the lattice parameter and the tetrahedral-oxygen and octahedral-oxygen bond lengths. Dashed lines are contours of constant lattice parameter (labeled in angstroms). Solid arrows show the observed variation in R_{tet} and R_{oct} during isothermal annealing at 923 K and $x = 0.75$. Dotted arrow shows the variation in R_{tet} and R_{oct} that would be caused by reduction of Fe^{3+} to Fe^{2+}.

TABLE 4. Changes in tetrahedral bond lengths and scattering lengths due to cation exchange

Forward cation exchange reaction	b_{tet} (fm)	R_{tet} (Å)*
$Fe^{3+}_{oct} + Fe^{2+}_{tet} = Fe^{3+}_{tet} + Fe^{2+}_{oct}$	constant (0)	decreases (–0.13)
$Fe^{3+}_{oct} + Mg_{tet} = Fe^{3+}_{tet} + Mg_{oct}$	increases (4.2)	decreases (–0.1)
$Fe^{3+}_{oct} + Al_{tet} = Fe^{3+}_{tet} + Al_{oct}$	increases (6.1)	increases (0.095)
$Fe^{2+}_{oct} + Mg_{tet} = Fe^{2+}_{tet} + Mg_{oct}$	increases (4.2)	increases (0.03)
$Fe^{2+}_{oct} + Al_{tet} = Fe^{2+}_{tet} + Al_{oct}$	increases (6.1)	increases (0.225)
$Mg_{oct} + Al_{tet} = Mg_{tet} + Al_{oct}$	increases (1.9)	increases (0.195)

*Number in brackets gives the change for the forward reaction.

High-temperature ordering behavior

The high-temperature cation ordering behavior of samples with $x = 0.4$ and 0.5 was investigated at temperatures between 873 and 1273 K. The high-temperature cation ordering behavior of the sample with $x = 0.75$ was investigated at temperatures between 923 and 1273 K, after isothermal annealing at 923 K for 4000 s (see previous section). All measurements were started at low temperature, and diffraction patterns were collected every 45 min during heating up to 1273 K (30 min collection time plus 15 min heating time). Measurements were made in 50 K steps for $x = 0.4$, 25 K steps for $x = 0.5$, and 15 K steps for $x = 0.75$. A limited number of diffraction patterns were collected during cooling, but evidence of exsolution began to appear at temperatures below 1073 K in samples with $x = 0.4$ and 0.5 (distinct broadening at the base of the diffraction peaks). No evidence of exsolution was detected during the heating experiments.

Figure 4 shows the variation of b_{tet} vs. T for the three samples studied. In all three cases the observed values of b_{tet} were greater than the hypothetical value associated with a completely disordered cation distribution (7.31 fm, 6.77 fm, and 5.43 fm for $x =$

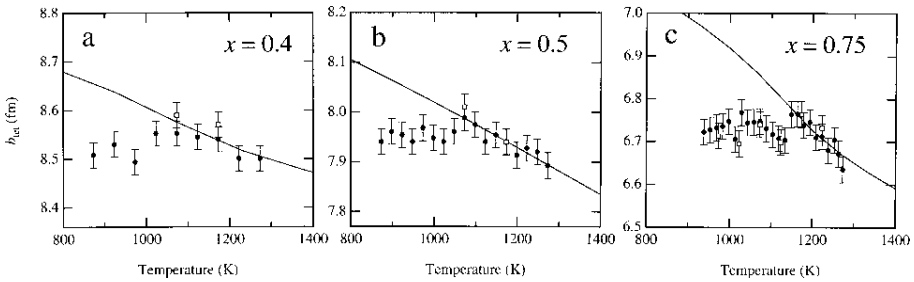

FIGURE 4. The tetrahedral scattering length, as a function of temperature for compositions (**a**) x = 0.4, (**b**) x = 0.5, and (**c**) x = 0.75. Solid lines show the proposed equilibrium variation in b_{tet} as a function of temperature. Solid symbols = measurements during heating. Open symbols = measurements during cooling.

0.4, 0.5, and 0.75, respectively). Therefore, a decreasing value of b_{tet} is associated with the system moving to a more disordered state (and vice versa). This behavior is characteristic of that seen in all non-convergent systems when quenched material is heated (Harrison and Putnis 1996; Harrison et al. 1998; Redfern et al. 1996; Sujata and Mason 1992). The starting value of b_{tet} is determined by the cation distribution obtained after quenching from 1673 K. This cation distribution is disordered with respect to the equilibrium cation distribution (indicated by the solid line), and hence there is a driving force for ordering as the material is heated. At low temperatures, the kinetics are too slow to allow ordering to occur, and b_{tet} remains constant. On heating to higher temperatures the rate of ordering increases, and the cation distribution begins to change. At some "relaxation temperature," T_r, the cation distribution rapidly approaches equilibrium. This is seen as the increase in b_{tet} onto the equilibrium curve at around 1073 K for x = 0.4 and 0.5, and at around 1140 K for x = 0.75. Above T_r the system begins to disorder. It may be assumed that the samples are at global equilibrium at temperatures above T_r. The maximum in b_{tet}, which occurrs at 1030 K in Figure 4c may be a non-equilibrium relaxation temperature, which occurs when a stage of intermediate equilibrium is approached on heating (similar to the effect seen during isothermal annealing of this sample). In this case, the decrease in b_{tet} between 1030 K and 1140 K corresponds to metastable disordering of the sample before global equilibrium is reached above T_r.

The corresponding variations in R_{tet} (Fig. 5) at temperatures below T_r are due mainly to thermal expansion. Above T_r there is an additional contribution due to the disordering cation distribution. This contribution is negative in all three cases, leading to a decrease in the slope of the R_{tet} vs. T curve. This allows a more accurate determination of T_r than using the scattering lengths themselves. This decrease is caused mainly by the exchange of Al cations onto tetrahedral sites, displacing the larger Mg and Fe^{2+} cations onto octahedral sites (Yamanaka and Takéuchi 1983).

Comparison with existing thermodynamic models

The $(Fe_3O_4)_{1-x}(MgAl_2O_4)_x$ solid solution is a ternary, which requires three parameters to fully describe the cation distribution:

$$Al_pFe^{3+}_qMg_rFe^{2+}_{1-p-q-r}\left[Al_{2x-p}Fe^{3+}_{2-2x-q}Mg_{x-r}Fe^{2+}_{p+q+r-x}\right]O_4. \qquad (2)$$

The neutron structure refinements provides two results (b_{tet} and R_{tet}) pertinent to the cation distribution. However, because in-situ values for the individual cation-oxygen bond lengths are unknown, R_{tet} cannot be used as a quantitative constraint. The measurements of b_{tet} can be used, however, to provide an empirical test of any given cation distribution model for the solid solution. Two models, of O'Neill and Navrotsky (1984) and Nell and Wood (1989), are discussed here.

The O'Neill and Navrotsky (1984) model is applicable to binary solid solutions. To reduce the $(Fe_3O_4)_{1-x}(MgAl_2O_4)_x$ solid solution to a binary, we assumed that Mg and Fe^{2+} had equal site preference energies (i.e., no partitioning of Mg relative to Fe^{2+} between tetrahedral and octahedral sites). This assumption is justified by the comparison of cation ordering in the end-members $MgAl_2O_4$, $FeAl_2O_4$, $MgFe_2O_4$, and Fe_3O_4 (Harrison et al. 1998; O'Neill et al. 1992; Wu and Mason 1981; Redfern et al. in preparation), and by the observation of ordering in the Fe_3O_4-$MgFe_2O_4$ solid solution (Nell et al. 1989). Under this assumption, the Mg and Fe^{2+} distributions are determined by the overall degree of inversion (p + q) and the bulk composition (x):

$$Al_pFe^{3+}_qMg_{x(1-p-q)}Fe^{2+}_{(1-x)(1-p-q)}\left[Al_{2x-p}Fe^{3+}_{2-2x-q}Mg_{x(p+q)}Fe^{2+}_{(1-x)(p+q)}\right]O_4. \qquad (3)$$

The free energy of the solid solution is given by combining the enthalpy change due to ordering with the configurational entropy:

$$\Delta G(p,q) = \alpha_{Al}p + \beta p^2 + \alpha_{Fe}q + \beta q^2 + 2\beta pq + RT\sum_{i,j} N_j X_i^j \ln X_i^j \qquad (4)$$

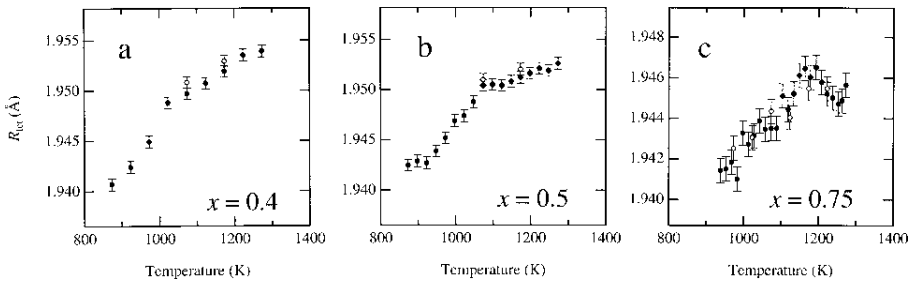

FIGURE 5. The tetrahedral-oxygen bond length as a function of temperature for compositions (**a**) x = 0.4, (**b**) x = 0.5, and (**c**) x = 0.75. Solid symbols indicate measurements during heating. Open symbols indicate measurements during cooling.

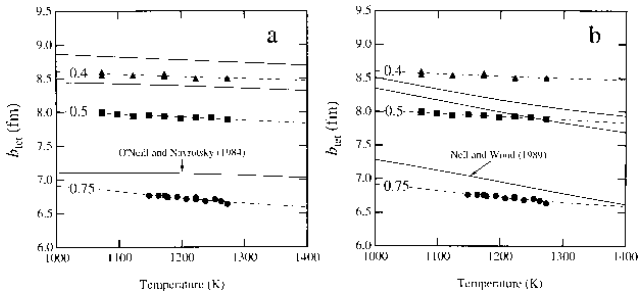

FIGURE 6. Comparison of observed tetrahedral scattering lengths, b_{tet} (fm), with values calculated using the thermodynamic models of (**a**) O'Neill and Navrotsky (1984) and (**b**) Nell and Wood (1989). Data points show the observed equilibrium values of b_{tet} for compositions $x = 0.4$ (triangles), 0.5 (squares), and 0.75 (circles). The size of the symbols indicates the uncertainty. Only the equilibrium data points measured at temperatures greater than T_r are shown. Solid lines indicate calculations using the thermodynamic models. Dashed lines indicate our proposed equilibrium variation in b_{tet} as a function of temperature.

where α_{Al}, α_{Fe}, and β are constants, x_j^i is the fraction of cation i on site j, and N_j is the number of j-sites per formula unit. O'Neill and Navrotsky (1983) argued that β is similar for all 2-3 spinels with an average value of $\beta = -20$ kJ/mol and obtained values of $\alpha_{Al} = 56$ kJ/mol and $\alpha_{Fe} = 20$ kJ/mol by fitting to the cation ordering behavior in the end-members. The equilibrium cation distribution is defined by the global minimum of Equation 4. This yields two equations that can be solved simultaneously to yield p and q. The full cation distribution is then calculated from Equation 3, and b_{tet} is calculated from the scattering lengths of the individual cations (Table 1).

Two main discrepancies occur between the curves calculated using the O'Neill and Navrotsky (1984) model and the results of our structure refinements (Fig. 6a). First, the magnitudes of the calculated scattering lengths are higher than observed. Second, the model predicts that for $x = 0.75$ the Fe^{3+} cations order onto the octahedral sites. This is contrary to our observation in the previous section that Fe^{3+} orders onto the tetrahedral site during isothermal annealing of this sample below T_r. However, good agreement exists between the observed and calculated slopes of the b_{tet} vs. T curves for the compositions $x = 0.4$ and 0.5.

The Nell and Wood (1989) model can be applied directly to the Mg-Al-Fe^{2+}-Fe^{3+} ternary solid solution without assuming similar properties for Mg and Fe^{2+}. The enthalpy due to ordering is formulated as a second-order Taylor expansion in the three cation distribution parameters and two compositional parameters required to fully describe the cation distribution. This is combined with the configurational entropy as before, and equilibrium is defined by the global minimum of the free energy with respect to the cation order parameters. This yields three equations that are solved simultaneously to give p, q, and r. There are 18 coefficients in the free energy expansion, which were determined by fitting to various cation ordering and phase equilibrium constraints. The predicted values of b_{tet} using this model (Fig. 6b) also agree poorly with observed scattering lengths for all three samples. In particular, the calculated slopes of the ordering curves are much greater than observed. As in the O'Neill and Navrotsky (1984) model, the Nell and Wood (1989) model predicts that Fe^{3+} orders onto octahedral sites for $x = 0.75$.

PROPOSED ORDERING SCHEME

Despite the limited temperature range over which equilibrium data were collected, the lack of agreement with the existing models suggests a need to re-examine the ordering behavior of the solid solution. To provide a more intuitive basis for comparing the observed data with the predictions of the thermodynamic models, we propose a possible cation ordering scheme that is consistent with the in-situ neutron refinements. We assume that Mg and Fe^{2+} have equal site preferences, which reduces the number of parameters describing the cation distribution to two (p and q). These parameters can be calculated by combining the measurements of b_{tet} with an additional experimental constraint, provided by measurements of saturation magnetization (M_s). In the majority of spinels, the magnetic moments associated with the Fe^{2+} and Fe^{3+} cations adopt a co-linear arrangement below the Curie temperature, with moments on tetrahedral sites aligned antiparallel to those on octahedral sites. In this case, the net saturation magnetization is given simply by the difference between the octahedral and tetrahedral sublattice magnetizations:

$$M_S = 2(\mu_{Fe3+}X^{oct}_{Fe3} + \mu_{Fe2+}X^{tet}_{Fe2+}) - \mu_{Fe3+}X^{tet}_{Fe3+} - \mu_{Fe2+}X^{tet}_{Fe2+} \quad (5)$$

where μFe^{3+} and μFe^{2+} are the 0 K magnetic moments of the Fe^{3+} and Fe^{2+} cations (5 μ_B and 4 μ_B respectively; 1 $\mu_B = 9.27 \times 10^{-24}$ Am^2).

There are two main problems involved in using measurements of M_s to constrain cation distributions. First, the measurements had to be made on quenched material, and hence there is the possibility that the disordered cation distribution is not maintained during quenching. This problem is serious for spinels containing Fe^{3+} and Fe^{2+}, because these cations can exchange rapidly with each other simply by the transfer of an electron. Second, we assume that the ideal collinear spin structure is adopted in all compositions of the solid solution. Although this is reasonable for magnetite-rich spinels, it becomes less certain when the magnetite component is diluted and the relative size of the inter- and intra-site magnetic interactions changes (Blasse 1964). If the assumptions are valid, measurements of M_s provided a precise and very sensitive constraint on the cation distribution. However, given the uncertainty regarding maintenance of the disordered Fe^{2+}-Fe^{3+} distribution during quenching, the following analysis is not quantitative. Our intention is to provide a qualitative picture of ordering in the solid solution.

For $T = 1173$ K, we used M_S determined by Harrison (1997) for the $(Fe_3O_4)_{1-x}(MgAl_2O_4)_x$ solid solution quenched from 1173 K using hysteresis loops measured at 4.4 K and in a maximum field of 12 T (Harrison and Putnis 1995, for experimental details). Values of $M_s = 1.32$, 0.88, and 0.025 μ_B were determined for samples with $x = 0.4$, 0.5, and 0.75 respectively. The cation distribution at other temperatures is derived from the b_{tet} data using the following fitting procedure. The variation of p and q as a function of temperature is calculated using the thermodynamic model of Carpenter et al. (1994). The starting values of the coefficients in the model were set equal to the values for the end-members $MgAl_2O_4$

and $MgFe_2O_4$ (Harrison and Putnis 1997; Redfern et al., in preparation). From this starting model, the corresponding variation in b_{tet} as a function of temperature is calculated and compared to the observed values. The coefficients in the thermodynamic model were then varied in a least squares procedure until the calculated b_{tet} curve best fit the observed data, and the values of p and q at 1173 K passed through those calculated from the M_s data. The use of the Carpenter et al. (1994) model to fit the data (and the values of the coefficients extracted) has little thermodynamic significance other than to ensure that p and q vary with temperature in a manner that is physically reasonable. No constraints on the cation distribution at 0 K were applied. The results of the fits are shown as the solid lines in Figure 4 and as the dashed lines in Figure 6.

In Figure 7, the solid lines show the tetrahedral cation occupancies extracted using the fitting procedure described above. The cation with the strongest site preference is Al, which occurs predominantly on octahedral sites in all three cases with a slowly increasing amount on tetrahedral sites at high temperatures. The ordering scheme adopted by the other cations is a compromise between the normal and inverse ordering schemes adopted in the end-members. According to the normal ordering observed in $MgAl_2O_4$, we expect Mg (and Fe^{2+}) to show a strong tetrahedral site preference relative to Al. According to the inverse ordering observed in Fe_3O_4, we expect Fe^{2+} (and Mg) to show an octahedral site preference relative to Fe^{3+}. In the solid solution, therefore, there is a conflict between placing Mg and Fe^{2+} cations on octahedral or tetrahedral sites. The simplest solution to this conflict is to distribute the cations randomly between those sites that are not already occupied by Al. This "pseudo-random" ordering scheme is indicated by the dashed lines in Figure 7. These lines were calculated by fixing the Al distribution equal to the Al distribution extracted from the fitting procedure, then distributing the other cation randomly over the remaining tetrahedral and octahedral sites. There is almost exact coincidence between this scheme and the fitted cation distribution for $x = 0.5$ (Fig. 7b). In the other two compositions, the overall values of the occupancies are also similar to the pseudo-random scheme at low temperatures. The fitted occupancies for these two compositions at higher temperatures is obtained by exchanging tetrahedral Fe^{3+} with octahedral Mg and Fe^{2+}, consistent with the Fe^{3+} tetrahedral site preference observed in the isothermal annealing experiment described earlier.

Figures 7b and 7c show the distributions of Fe^{2+} and Fe^{3+} (Nell et al. 1989) using the in-situ electrical conductivity/Seebeck-effect technique (Mason 1987). For both compositions there is reasonable agreement between the observed Fe^{2+} (Nell et al. 1989) and the fitted Fe^{2+} distribution of this study. There is, however, a large discrepancy between the Fe^{3+} distributions. This discrepancy is also evident from the saturation magnetization measurements. From the data of Nell et al. (1989), we calculated average saturation magnetizations of $M_s = -1.38\ \mu_B$ and $-2.65\ \mu_B$ for $x = 0.5$ and 0.75, respectively (Eq. 6). These differ from observed values of $M_s = 0.88\ \mu_B$ and $0.025\ \mu_B$ (Harrison 1997), indicating that the measurements of Nell et al. (1989) overestimated the amount of Fe^{3+} on tetrahedral sites.

DISCUSSION

The calculated slope in b_{tet} with T (Fig. 6) is very different for the O'Neill and Navrotsky (1984) and Nell and Wood (1989) models, and the slopes calculated with the O'Neill and Navrotsky (1984) model are very similar to the observed slopes for $x = 0.4$ and 0.5. The reason for this can now be investigated by comparing the calculated cation occupancies for the two thermodynamic models with our proposed cation ordering scheme.

The solid lines in Figure 8a show the calculated behavior using the O'Neill and Navrotsky (1984) model for the composition $x = 0.5$. The dashed lines show the ordering scheme from this study, obtained by fitting to b_{tet} and M_s. The two ordering schemes are very similar, both being almost exactly described by the pseudo-random scheme. For example, taking the Al distribution calculated by the O'Neill and Navrotsky (1984) model, we see that at 800 K the 1 Al cation pfu resides exclusively on octahedral sites. The 1 Fe^{3+}, 0.5 Fe^{2+}, and 0.5 Mg cations pfu are then distributed randomly over the remaining two sites, yielding tetrahedral occupancies of 0.5 Fe^{3+}, 0.25 Fe^{2+}, and 0.25 Mg. According to the pseudo-random scheme, the temperature dependence of the cation distribution as a whole is controlled by the rate of exchange of Al between sites. Because only small amounts of Al disorder onto tetrahedral sites, the temperature dependence of the cation distribution in the solid solution is greatly reduced. This is responsible for the very small slopes of the calculated b_{tet} curves in Figure 6a.

Less similarity exists between the Nell and Wood (1989) model and our proposed ordering scheme (Fig. 8a). This model predicts a pronounced temperature dependence of the Fe^{3+} distribution, which is responsible for the steep slope of the calculated b_{tet} curves in Figure 6b.

We conclude that our structure refinements are broadly consistent with the thermodynamic model of O'Neill and Navrotsky (1984) for compositions close to the center of the solid solution. At this composition, the conflict between the normal and inverse ordering schemes is greatest, leading to a compromise distribution with very little change in the cation occupancies as a function of temperature. The small magnitude of the changes in b_{tet} ob-

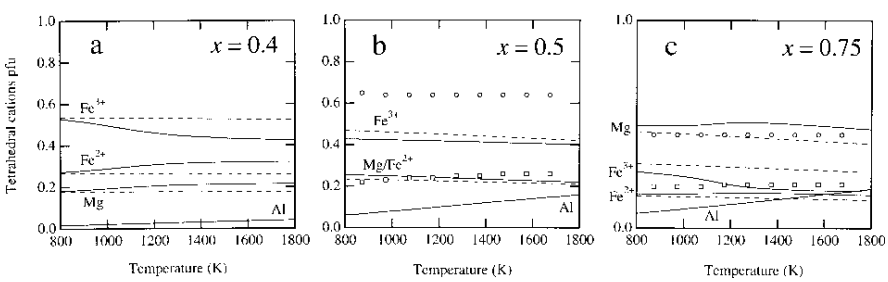

FIGURE 7. Proposed tetrahedral site occupancies as a function of temperature in compositions (**a**) $x = 0.4$, (**b**) $x = 0.5$, and (**c**) $x = 0.75$. Solid lines indicate occupancies obtained by fitting to the in-situ b_{tet} data and the quench magnetization data. Dashed lines indicate occupancies that would be obtained by distributing Mg, Fe^{2+}, and Fe^{3+} randomly between the sites not occupied by Al. The data points in **b** and **c** show the distributions of Fe^{3+} (circles) and Fe^{2+} (squares) determined by Nell et al. (1989).

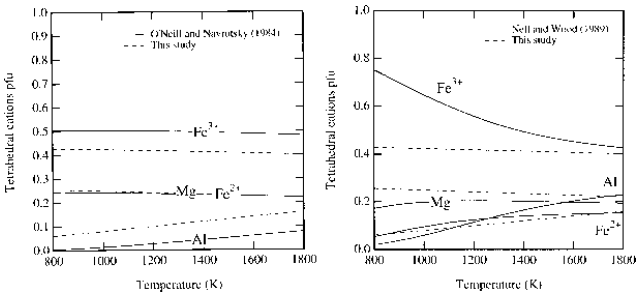

FIGURE 8. Comparison of tetrahedral site occupancies calculated by (**a**) O'Neill and Navrotsky (1984) and (**b**) Nell and Wood (1989) (solid lines), with the proposed cation distribution from this study (dashed lines).

served for all three samples here suggest that this simple ordering scheme provides the template for ordering over a range in compositions about the middle of the solid solution. More in-situ experiments are now required to determine how close to the end-members this template is valid. Although the temperature dependence of the cation distribution predicted by the O'Neill and Navrotsky (1984) model is in agreement with the structure refinements, a large discrepancy exists between the magnitude of the observed and calculated scattering factors (Fig. 6a). The explanation for this could lie in the assumption that $\beta = -20$ kJ/mol is a universal constant for 2-3 spinels. Recent in-situ neutron structure refinements on the end-members $FeAl_2O_4$ and $MgAl_2O_4$ (Harrison et al. 1998; Redfern et al., in preparation) strongly challenge this assumption and suggest that in these materials β has the opposite sign to that observed in other 2-3 spinels. In this case, the O'Neill and Navrotsky (1984) model would require significant revision before applying it to the Mg-Fe-Al spinel system.

ACKNOWLEDGMENTS

R.J.H. gratefully acknowledges the financial support of the Alexander von Humbold-Stiftung and the Deutsche Forschungsgemeinshaft. We thank R.C. Peterson, A. Navrotsky, and A. Poustovetov for their reviews of the manuscript, and H.St.C. O'Neill for his helpful comments on an earlier version.

REFERENCES CITED

Blasse, G. (1964) Crystal chemistry and some magnetic properties of mixed metal oxides with spinel structure. Philips Research Reports Supplements, 3, 1–139.

Carpenter, M.A., Powell, R.A., and Salje, E.K.H. (1994) Thermodynamics of nonconvergent cation ordering in minerals: I. An alternative approach. American Mineralogist, 79, 1053–1067.

Dieckmann, R. (1982) Defects and cation diffusion in magnetite IV: Non-stoichiometry and point defect structure of magnetite ($Fe_{3-\delta}O_4$). Berichte Bunsengesellschaft Physikalische Chemie, 86, 112–118.

Harrison, R.J. (1997) Magnetic properties of the magnetite-spinel solid solution. Ph.D. thesis. University of Cambridge, U.K.

Harrison, R.J. and Putnis, A. (1995) Magnetic properties of the magnetite-spinel solid solution: Saturation magnetization and cation distributions. American Mineralogist, 80, 213–221.

——(1996) Magnetic properties of the magnetite-spinel solid solution: Curie temperatures, magnetic susceptibilities and cation ordering. American Mineralogist, 81, 375–384.

——(1997) The coupling between magnetic, and cation ordering: a macroscopic approach. European Journal of Mineralogy, 9, 1115–1130.

Harrison, R.J., Redfern, S.A.T., and O'Neill, H.St.C. (1998) The temperature dependence of the cation distribution in synthetic hercynite ($FeAl_2O_4$) from in-situ neutron structure refinements. American Mineralogist, 83, 1092–1099.

Larsson, L., O'Neill, H.St.C., and Annersten, H. (1994) Crystal chemistry of the synthetic hercynite ($FeAl_2O_4$) from XRD structural refinements and Mössbauer spectroscopy. European Journal of Mineralogy, 6, 39–51.

Lehmann, J. and Roux, J. (1984) Calculations of activity-composition relations in multisite solid solutions: the example of AB_2O_4 spinels. Contributions to Mineralogy and Petrology, 87, 328–336.

Mason, T.O. (1987) Cation intersite distributions in iron-bearing minerals via electrical conductivity/seebeck effect. Physics and Chemistry of Minerals, 14, 156–162.

Millard, R.L., Peterson, R.C., and Hunter, B.K. (1992) Temperature dependence of cation disorder in $MgAl_2O_4$ spinel using ^{27}Al and ^{17}O magic-angle spinning NMR. American Mineralogist, 77, 44–52.

Nafziger, R.H., Ulmer, G.C., and Woermann, E. (1971) Gaseous buffering for the control of oxygen fugacity at one atmosphere pressure. In G. C. Ulmer , Ed., Research Techniques for High Pressure and High Temperature. Springer-Verlag, New York.

Nell, J. and Wood, B.J. (1989) Thermodynamic properties in a multi-component solid solution involving cation disorder: in Fe_3O_4-$MgFe_2O_4$-$FeAl_2O_4$-$MgAl_2O_4$ spinels. American Mineralogist, 74, 1000–1015.

Nell, J., Wood, B.J., and Mason, T.O. (1989) High-temperature cation distribution in Fe_3O_4-$MgFe_2O_4$-$FeAl_2O_4$-$MgAl_2O_4$ spinels from thermopower and conductivity measurements. American Mineralogist, 74, 339–351.

O'Neill, H.St.C. (1994) Kinetics of cation order-disorder in $MgFe_2O_4$ spinel. European Science Foundation Program on Kinetic Processes in Minerals and Ceramics, proceedings of a workshop on kinetics of cation ordering, Cambridge, England.

O'Neill, H.St.C. and Navrotsky, A. (1983) Simple spinels: crystallographic parameters, cation radii, lattice energies, and cation distribution. American Mineralogist, 68, 181–194.

——(1984) Cation distributions and thermodynamic properties of binary spinel solid solutions. American Mineralogist, 69, 733–753.

O'Neill, H.St.C. and Wall, V.J. (1987) The olivine-orthopyroxene-spinel oxygen goebarometer, the nickel precipitation curve, and the oxygen fugacity of the Earth's upper mantle. Journal of Petrology, 28, 1169–1191.

O'Neill, H.St.C., Annersten, H., and Virgo, D. (1992) The temperature dependence of the cation distribution in magnesioferrite ($MgFe_2O_4$) from powder XRD structural refinements and Mössbauer spectroscopy. American Mineralogist, 77, 725–740.

Peterson, R.C., Lager, G.A., and Hitterman, R.L. (1991) A time-of-flight powder diffraction study of $MgAl_2O_4$ at temperatures up to 1273 K. American Mineralogist, 76, 1455–1458.

Redfern, S.A.T., Henderson, C.M.B., Wood, B.J., Harrison, R.J., and Knight, K.S. (1996) Determination of olivine cooling rates from metal-cation ordering. Nature, 381, 407–409.

Sack, R.O. and Ghiorso, M.S. (1991) An internally consistent model for the thermodynamic properties of Fe-Mg-Titanomagnetite-aluminate spinels. Contributions to Mineralogy and Petrology, 106, 474–505.

Sha, L. and Chappell, B.W. (1996) Two-site multi-cation ordering-disordering in minerals: an alternative kinetic model. American Mineralogist, 81, 881–890.

Sujata, K. and Mason, T.O. (1992) Kinetics of cation redistribution in ferrospinels. Journal of the American Ceramic Society, 75, 557–562.

Wood, B.J. (1990) An experimental test of the spinel peridotite oxygen barometer. Journal of Geophysical Research-Solid Earth and Planets, 95, 15845–15851.

Wood, B.J., Kirkpatrick, R.J., and Montez, B. (1986) Order-disorder phenomena in $MgAl_2O_4$ spinel. American Mineralogist, 71, 999–1006.

Woodland, A.B. (1988) Fe-Ti and Fe-Al oxides as indicators of oxygen fugacity in rocks. Ph.D. thesis, Northwestern University, Evanston, IL.

Wu, C.C. and Mason, T.O. (1981) Thermopower measurement of cation distribution in magnetite. Journal of the American Ceramic Society, 64, 520–522.

Yamanaka, T. and Takéuchi, Y. (1983) Order-disorder transition in $MgAl_2O_4$ spinel at high temperatures up to 1700 DEGC. Zeitschrift für Kristallographie, 165, 65–78.

MANUSCRIPT RECEIVED NOVEMBER 20, 1997
MANUSCRIPT ACCEPTED OCTOBER 30, 1998
PAPER HANDLED BY RONALD C. PETERSON